MRS Advances

Optical design of perovskite solar cells for applications in monolithic tandem configuration with $CuInSe_2$ bottom cells

Ramez H. Ahangharnejhad, Zhaoning Song, Adam B. Phillips, Suneth C. Watthage, Zahrah S. Almutawah, Dhurba R Sapkota, Prakash Koirala, Robert W. Collins, Yanfa Yan, Michael J. Heben

Department of Physics and Astronomy, University of Toledo, Toledo, Ohio 43606, United States

Wright Center for Photovoltaics Innovation and Commercialization, Toledo, Ohio 43606, United States

Abstract:

Monolithic integrated thin film tandem solar cells consisting of a high bandgap perovskite top cell and a low bandgap thin film bottom cell are expected to reach higher power conversion efficiencies (PCEs) with lower manufacturing cost and environmental impacts than the market-dominant crystalline silicon photovoltaics. There have been several demonstrations of 4-terminal and 2-terminal perovskite tandem devices with $CuInGaSe_2$ (CIGS) or $CuInSe_2$ (CIS) and, similar to the other tandem structures, the optimization of this device relies on optimal choice for the perovskite bandgap and thickness. Therefore, further advancement will be enabled by tuning the perovskite absorber to maximize the photocurrent limited by the current match condition. Here, we systematically study the optical absorption and transmission of perovskite thin films with varying absorber band gap. Based on these results, we model the photocurrent generations in both perovskite and CIS subcells and estimate the performances of projected tandem devices by considering the ideally functioning perovskite and CIS device. Our results show that for perovskite layers with 500 nm thickness the optimal bandgap is around 1.6 eV. With these configurations, PCEs above 20% could be achieved by monolithically integrated perovskite/CIS tandem solar cells. Also by modelling the absorption at every layer we calculate the quantum efficiency at each subcell in addition to tracking optical losses.

INTRODUCTION

Combining narrow and wide bandgap semiconducting photovoltaic devices in a tandem structure has been regarded as the most effective method to overcome the theoretical limitation on power conversion of photovoltaic devices known as Shockley–Queisser limit [1]. However, the combination of top and bottom cells have to be optimized in terms of performance to produce highly efficient tandem structure. So far the most efficient demonstrations of tandem devices have been with III-V groups semiconductors as top cell and crystalline Si bottom cells [2]. Additionally, attempts to produce high efficiency devices with perovskite top cell and crystalline silicon bottom cell have been made [3]. Perovskite devices have been regarded as the most versatile choice for the top cell of the tandem devices since the fabrication of perovskite cells, using solution processes with short, low temperature heat treatments, is unlikely to damage the bottom cell. Also the bandgap engineering of perovskite devices is achievable with variations in the chemical compositions of the precursor solutions [4] which allows for simple optimization of the overall tandem device performance.

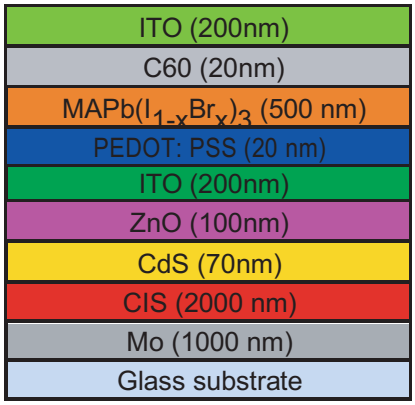

Figure 1. The design structure of the 2-terminal perovskite/CIS tandem device

In addition to developing devices that can surpass the most basic limitations associated with the PV technology, tandem cells can also offer an avenue for high efficiency devices that have lower cost and environmental impacts. Recent studies have shown that the cost of production of perovskite/perovskite or perovskite/CIGS based tandem devices can be lower than the single junction silicon devices while being an environmentally friendly option [5-7]. Out of these two options, perovskite/CIGS is the more viable route for efficient PV devices with low cost and low environmental impact as the narrow bandgap perovskite cells deployed as the bottom cell of the tandem cells have low lifetime [8]. Also with the possibility of fabricating CIGS devices using solution processed methods [9] this tandem structure may eventually be produced with print based fabrication techniques.

Despite efforts to fabricate perovskite/CIGS tandem devices, determination of the optimized structure for the best performance of this device remains elusive. An important step in optimizing the tandem device performance is to determine the current matching condition for the top and bottom cells. In this work, we have investigated the optimal choice for the bandgap of the perovskite film to satisfy the current matching condition and have calculated the device performance as for variable perovskite structure.

OPTICAL PROPERTIES OF THE LAYERS

Figure 1 shows an illustration of the two terminal perovskite/CIS device structure used in this work. The perovskite cell follows the inverted design to form a compatible structure with the CIS device in substrate configuration. The top cell consists of electron and hole transport layers (ETL and HTL) above and below the perovskite layer, respectively. Several materials have been proposed for these transport layers. For solution processed devices typical ETL choices have included Phenyl-C61-butyric acid methyl ester (PCBM) [10] or inorganic options such as ZnO [11]. On the other hand, high efficiency devices have been demonstrated with thermally evaporated C60 fullerene layer as the ETL [12]. For the HTL layer, the typical materials used for inverted structure of perovskite have included poly(3,4-ethylenedioxythiophene):polystyrene sulfonate (PEDOT:PSS) [13], Poly(triaryl amine) (PTAA) [14] or NiO [11]. This cell has ITO front and back contacts, whereas the bottom CIS cell has ITO and Molybdenum front and back contacts with ZnO/CdS ETLs. Thicknesses considered for every layer are taken from the literature [12,15] as are the refractive indices for ITO [16], C60 [17], MgF_2 [18] and PEDOT:PSS [19,20].

For the purpose of this work, perovskite thin films were prepared by spin coating 1M precursor solution with respective stoichiometry in DMF and DMSO (4:1 volume ratio). The spin coating procedure was performed with 1000 and 4000 rpm speed for 5 and 25 seconds, respectively. 550 μl diethyl ether anti-solvent was injected 3 seconds into the second step of the spin coating and the resultant thin films were annealed at 100 °C hot plate for 6 minutes. The refractive indices were measured using ellipsometry. Preliminary analysis was performed to determine the refractive indices of these films. These results indicate bandgaps of 1.57, 1.62, 1.67 and 1.73 eV for the stoichiometric values of x = 0, 0.1, 0.2 and 0.3, respectively, in $MAPb(I_{1-x}Br_x)_3$. Similar analyses were performed for the CIS thin films deposited with co-evaporation of Cu, In, Se with a Cu to In ratio of 1. Refractive indices for the remaining layers associated with the CIS structure have been reported [15].

METHOD

To model the current generation for the tandem structure, the transfer matrix method was used. To apply this method, an algorithm was developed following the theoretical description by Pettersson et al [17] and model developed by Burkhard et al [21]. Here, the work from Burkhard et al was expanded to treat the transverse electric or s-polarization (TE) and transverse magnetic or p-polarized (TM) separately, which allows for the consideration of angular refraction at each interface.

Following Pettersson et al work, the algorithm involves calculating two sets of scattering matrices for the layers stacked above (S') and below (S'') the absorber layer where the current generation (or optical losses) occurs as described by following equations:

$$S' = \left(\prod_{n=1}^{j-1} I_{(n-1)n} L_n \right) . I_{(j-1)j} \tag{1a}$$

$$S'' = \left(\prod_{m=j+1}^{k-1} I_{(m-1)m} L_m \right) . I_{(k-1)k} \tag{1b}$$

where j is the index of the absorber layer and k is the total number of the layers in the device stack. I_{xy} and L_y describe the reflection and transmission at every interface and the absorption of the light propagating through the layer and are referred to as the interface matrix and the propagation matrix, respectively. These matrices are calculated as

$$I_{xy} = {}^{1}/_{t_{xy}} \begin{bmatrix} 1 & r_{xy} \\ r_{xy} & 1 \end{bmatrix} \tag{2a}$$

$$L_Y = \begin{bmatrix} e^{\frac{-(2\pi i)\tilde{n}_y d_y \cos\theta_y}{\lambda}} & 0 \\ 0 & e^{\frac{(2\pi i)\tilde{n}_y d_y \cos\theta_y}{\lambda}} \end{bmatrix} \tag{2b}$$

where $\tilde{n}_y$, d_y, θ_y are the complex refractive index, the path length of the light, and the refraction angle of the layer, respectively, with identification index y and λ is the wavelength of the light. t_{xy} and r_{xy} are the transmission and reflection coefficients at the xy interface. By considering the refraction angle at every interface, the method developed for this work is an extension to the model built by Burkhard et al. By including the angular dependence t_{xy} and r_{xy} values are polarization dependent and they should be calculated separately for the TE and TM polarizations:

$$t_{xy,TE} = \frac{2\tilde{n}_x \cos\theta_x}{\tilde{n}_y \cos\theta_y + \tilde{n}_x \cos\theta_x} \tag{3a}$$

$$t_{xy,TM} = \frac{2\tilde{n}_x \cos\theta_x}{\tilde{n}_y \cos\theta_x + \tilde{n}_x \cos\theta_y} \tag{3b}$$

$$r_{xy,TE} = \frac{\tilde{n}_x \cos\theta_x - \tilde{n}_y \cos\theta_Y}{\tilde{n}_x \cos\theta_x + \tilde{n}_y \cos\theta_y} \tag{3c}$$

$$r_{xy,TM} = \frac{\tilde{n}_x \cos\theta_x - \tilde{n}_y \cos\theta_y}{\tilde{n}_x \cos\theta_y + \tilde{n}_y \cos\theta_x} \tag{3d}$$

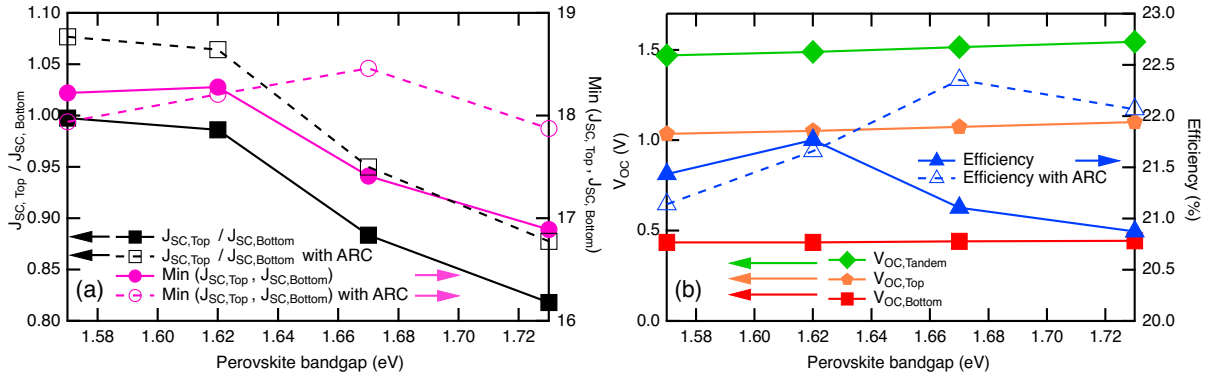

Figure 2. (a) Ratio of the current generated at the top perovskite cell to bottom CIS cell and minimum generated current at the either top perovskite or bottom CIS cell. (b) Top perovskite, bottom CIS and total tandem cell V_{OC}. Both panels are shown as a function of perovskite film bandgap.

The scattering matrix set described above are used to calculate the internal electric field at any given cross section (d) of the absorber layer

$$E_j(d) = \frac{S''_{j\,11}e^{-(2\pi i)\tilde{n}_j(d_y-d)\cos\theta_y} + S''_{j\,21}e^{(2\pi i)\tilde{n}_j(d_y-d)\cos\theta_y}}{S'_{j\,11}S''_{j\,11}e^{-(2\pi i)\tilde{n}_j(d_j-d)\cos\theta_y} + S'_{j\,11}S''_{j\,21}e^{(2\pi i)\tilde{n}_j(d_j-d)\cos\theta_y}} E_0^+ \quad (4)$$

where E_0^+describes the intensity of the field transmitted at the first interface and can be varied be by considering different values for the air mass. The carrier generation rate is calculated with

$$Q_j(d) = \frac{2\pi c\epsilon_0}{\lambda} Im(\tilde{n}_j)Re(\tilde{n}_j)\left|E_j(d)\right|^2 \quad (5)$$

where c and ϵ_0 are the speed of light and the permittivity of the vacuum, respectively. Using the generation rate, the current is calculated by summing over the thickness of the absorber layer slab. For the calculations performed for this work all the interfaces are considered to be optically flat and the internal quantum efficiency of the device was taken as 100%. AM 1.5 spectrum is used as the incident light spectrum.

RESULTS

The transfer matrix method was applied to calculate the current generated at the perovskite and CIS layers (see Figure 1) while the composition of the perovskite layer was varied as previously described. The thickness value for the perovskite layer was considered to be 500 nm. The generated current ratio of the perovskite device to the CIS device is given in Figure 2 (a) as a function of the perovskite bandgap. As shown in the figure the current matching is achieved for the perovskite with a bandgap of 1.57 eV, which does not have any Br content. For the case of perovskite film with a bandgap of 1.62 eV (x = 0.9 in $MAPb(I_{0.9}Br_{0.1})_3$) a near current matching condition is realized with a ratio of generated current at top cell to bottom slightly lower than one. For wider bandgap perovskite this ratio further decreases.

For devices with anti-reflection coating (ARC), 50 nm MgF_2 layer was introduced on top of the device stack and the optical analysis was completed to calculate the current generated at each subcell and also the ratio of current at top to bottom subcells. The ratio, shown in figure2 (a), indicate higher current generated in the top perovskite cells for narrow side of the studied bandgap range (1.59 eV and 1.62 eV). For higher bandgaps (1.67 eV and 1.73 eV) the bottom CIS subcell produces

higher currents. Assuming a linear trend, the current matching condition would be expected for 1.64 eV bandgap perovskite top cell.

In monolithically integrated tandem devices, when the current matched condition is met, the current generated in each subcell is the same and equal to the overall current of the tandem device. For devices that do not meet this condition, the overall current of the tandem cell corresponds to the minimum current generated in either top or bottom device [22]. Devices in this condition were also investigated by determining the minimum current generated in either the top or bottom cell. Figure 2 (a) also shows the results of the minimum current generated in either the top or bottom cell. As expected from the results of current ratio from top to bottom cell, the minimum generated current corresponds to the top cell for the wide bandgap perovskite cells. The results indicate that optimal overall current is slightly higher than 18 mA/cm^2 which is realized in the current matched devices. For results with ARC the highest tandem current is slightly higher.

To predict the overall efficiency of the tandem cell, the open circuit voltage approximations were considered for both subcells. The V_{OC} of the bottom cell was calculated using the following equation [23]

$$V_{OC}(P) = C + \frac{nkT}{q}\ln(P) \tag{6}$$

where P is the normalized power density to the overall power density of the AM1.5 spectrum. C is the open circuit voltage at maximum incident power. k, T, q are the Boltzmann constant, temperature, elementary charge, respectively, and n is the ideality factor. The incident power dependence of the ideality factor was taken from literature [24]. To calculate the incident power density dependent V_{oc} of the CIS cell, the spectrum of the incident power was calculated using the device stack shown in Figure 1, with the appropriate perovskite material, and the transfer matrix method. The incident power density on the CIS layer was derived from integration of the transmitted AM 1.5 spectrum. The standard V_{oc} for the CIS cell (formulated as C in the equation) was taken as 0.5 V [25]. The bottom cell V_{OC} is plotted in Figure 2 (b). The values of the V_{oc} do not vary greatly from the one of unfiltered illumination condition.

For the top cell, the open circuit voltage of the standard inverted perovskite device was calculated from the bandgap dependence of optimized devices [4]. The top cell V_{OC} is also plotted in Figure 2 (b). The overall tandem V_{OC} was calculated as the sum of the top and bottom cell Voc. The overall tandem cell V_{OC} is around 1.5 V for the perovskite bandgap range investigated here.

To calculate the overall efficiency of the tandem device, a fill factor of 80% was assumed, and the J_{SC} and V_{OC} values presented in Figure 2 (a) and 2 (b) were used. The efficiency of the 2 terminal perovskite/CIS tandems as a function of the

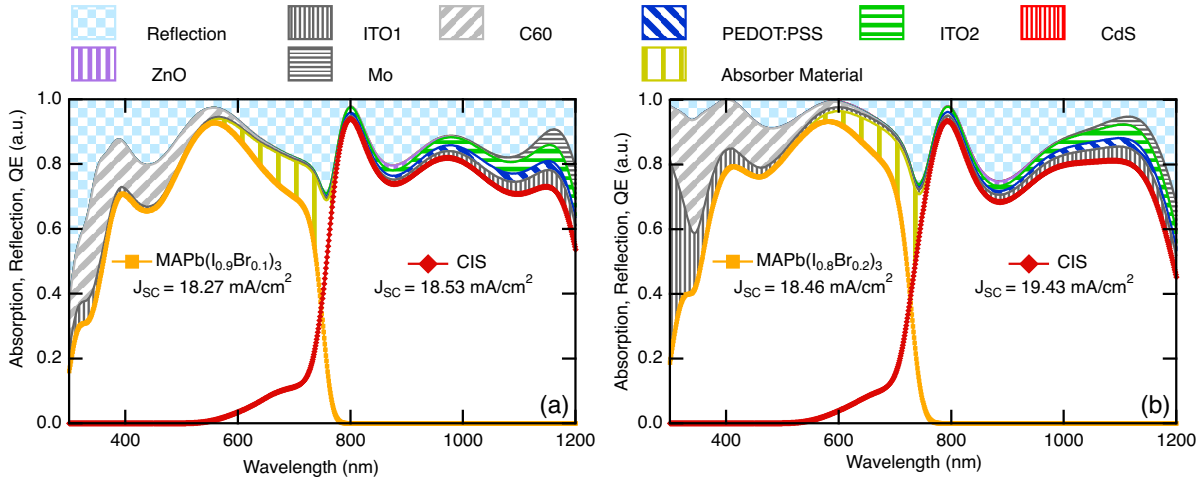

Figure 3. Quantum efficiency of the perovskite and CIS devices, absorption spectrum of the layers other than absorber material and the reflection spectrum calculated for the tandem device with 500 nm thickness perovskite with (a) 1.62 eV bandgap and $MAPb(I_{0.9}Br_{0.1})_3$ perovskite composition and (b) 1.67 eV bandgap $MAPb(I_{0.8}Br_{0.2})_3$ perovskite composition. Device stack in panel (b) contains AR coating.

perovskite composition show that the highest expected efficiency of above 21% can be achieved with 500 nm thick perovskite film with 1.62 eV bandgap or $MAPb(I_{0.9}Br_{0.1})_3$ composition. With addition of ARC the optimal efficiency for the tandem structure is above 22%. This can be achieved with 1.67 eV bandgap or $MAPb(I_{0.8}Br_{0.2})_3$ composition.

To identify the dissipations across the incident spectrum, quantum efficiency simulations of the tandem device were generated. Figure 3 (a) shows the results of the simulations for tandem device with $MAPb(I_{0.9}Br_{0.1})_3$ perovskite composition. This structure is associated with the tandem device with highest expected device efficiency. The QE of each absorber layer is outlined with orange (for perovskite) and red (for CIS) devices. The summation of the QE profiles for both cells are shown as absorber layer. The absorption in each layer is shown with shaded regions. The dissipation in lower wavelength range of the spectrum is mostly associated with the C60 transport layer in the top perovskite cell. The current dissipation in this layer is equivalent to 1.2 mA/cm^2. The front contact and tunnel junction ITO layers are responsible for current losses of 0.75 mA/cm^2 and 0.5 mA/cm^2, respectively. Current losses in CdS, which is typically ~2 mA/cm^2 in single junction CIS devices, is negligible due to short wavelength absorption in the top cell. The calculated current loss correlated with the absorption in PEDOT:PSS and ZnO layers were 0.38 and 0.1 mA/cm^2, respectively, while the Mo back contact accounts for 0.22 mA/cm^2. The development of this model will allow each of these layers to be varied to determine the optimum device configuration and layer thicknesses. Figure 3 (b) shows the QE simulation for the device with highest expected efficiency for tandem device with ARC. Generated currents are improved for both subcells with addition of ARC and losses to reflection are reduced.

CONCLUSION

To study the performance of the perovskite/CIS tandem structure, a model based on the transfer matrix method was developed. The model was set in a way to treat the TE and TM polarizations of the incident light separately to include the refraction into the transmission, reflection and absorption of the light. To perform the studies with the model, refractive index library was generated using the previously reported data. For the perovskite layers, thin films were deposited by spin coating and studied with ellipsometry. The refractive indices from preliminary results indicated bandgap variations between 1.57 eV and 1.73 eV. Using the refractive index library, the current generated in both subcells of the tandem device were calculated. These values were used to derive the overall tandem short circuit current density and the current matching condition. The V_{OC} of each subcell was also calculated to estimate the total tandem device V_{OC}. For the top cell, the bandgap dependence of the V_{OC} was adapted from literature, and for the bottom cell a model based on the incident light intensity was developed. Using the calculated V_{OC} and J_{SC} values device performances were calculated for the 80% fill factor. For the studied range of perovskite options, optimal device has efficiency of 21% this value can be increased to above 22% with addition of ARC. EQE results were also generated and show where the current losses occur. Using this model higher efficiency devices can be designed by tailoring each layer thickness.

ACKNOWLEDGMENTS

This work was supported in part by the National Science Foundation (ECCS-1665172) and in part by the Office of Naval Research (N00014-17-1-2223).

References

1. A. De Vos, *J. Phys. D* **13**, 839–846 (1980).
2. S. Essig, C. Allebé, T. Remo, J. F. Geisz, M. A. Steiner, K. Horowitz, L. Barraud, J. S. Ward, M. Schnabel, A. Descoeudres, D. L. Young, M. Woodhouse, M. Despeisse, C. Ballif and A. Tamboli, *Nat. Energy* **2**, 17144 (2017).
3. J. Werner, C. H. Weng, A. Walter, L. Fesquet, J. P. Seif, S. De Wolf, B. Niesen and C. Ballif, *J. Phys. Chem. Lett.*, **7**, 161–166 (2016).
4. J. Werner, G. Nogay, F. Sahli, C. T. Yang, G. Christmann, A. Walter, B. Kamino, P. Fiala, S. Nicolay, Q. Jeangros, B. Niesen and C. Ballif, *ACS Energy Lett.* **12 (1)**, 876–883 (2018).
5. I. Celik, A. B. Phillips, Z. Song, Y. Yan, R. J. Ellingson, M. J. Heben and D. Apul, *Energy Environ. Sci.* **10**, 1874–1884 (2017).
6. I. Celik, A. B. Philips, Z. Song, Y. Yan, R. J. Ellingson, M. J. Heben and D. Apul, *IEEE J. Photovoltaics* **8**, 305–309 (2018).
7. Z. Song, C. L. McElvany, A. B. Phillips, I. Celik, P. W. Krantz, S. C. Watthage, G. K. Liyanage, D. Apul and M. J. Heben, *Energy*

Environ. Sci **10**, 1297–1305 (2017).
8. D. Zhao, Y. Yu, C. Wang, W. Liao, N. Shrestha, C. R. Grice, A. J. Cimaroli, L. Guan, R. J. Ellingson, K. Zhu, X. Zhao, R.-G. Xiong and Y. Yan, *Nat. Energy* **2**, 17018 (2017).
9. Y. S. Lim, H. S. Kwon, J. Jeong, J. Y. Kim, H. Kim, M. J. Ko, U. Jeong and D. K. Lee, *ACS Appl. Mater. Interfaces* **6**, 259–267 (2014).
10. D.-X. Yuan, X.-D. Yuan, Q.-Y. Xu, M.-F. Xu, X.-B. Shi, Z.-K. Wang and L.-S. Liao, *Phys. Chem. Chem. Phys.* **17**, 26653–26658 (2015).
11. J. You, L. Meng, T. Song, T. Guo, Y. M. Yang, W. Chang, Z. Hong, H. Chen, H. Zhou, Q. Chen, Y. Liu and N. De Marco, Yang Yang, *Nat. Nanotechnol.* **11**, 75–81 (2016).
12. D. Zhao, C. Wang, Z. Song, Y. Yu, C. Chen, X. Zhao, K. Zhu and Y. Yan, *ACS Energy Lett.* **3 (2)**, 305–306 (2018).
13. J. H. Heo, H. J. Han, D. Kim, T. K. Ahn and S. H. Im, *Energy Environ. Sci.* **8**, 1602–1608 (2015).
14. J. H. Heo, S. H. Im, J. H. Noh, T. N. Mandal, C. S. Lim, J. A. Chang, Y. H. Lee, H. J. Kim, A. Sarkar, M. K. Nazeeruddin, M. Grätzel and S. Il Seok, *Nat. Photonics* **7**, 486–491 (2013).
15. A. R. A. Ibdah, P. Koirala, P. Aryal, P. Pradhan, M. J. Heben, N. J. Podraza, S. Marsillac and R. W. Collins, *J. Energy Chem.* **2095** 4956, (2017).
16. T. A. F. Konig, P. A. Ledin, J. Kerszulis, M. A. Mahmoud, M. A. El-sayed, J. R. Reynolds and V. V Tsukruk, *ACS Nano* **8**, 6182–6192 (2014).
17. L. A. A. Pettersson, L. S. Roman and O. Inganäs, *J. Appl. Phys.* **86**, 487–496 (1999).
18. L. V. Rodríguez-de Marcos, J. I. Larruquert, J. A. Méndez, J. A. Aznárez, *Opt. Exp.***7 (3)**, 989-1006 (2017).
19. J. Gasiorowski, R. Menon, K. Hingerl, M. Dachev and N. S. Sariciftci, *Thin Solid Films* **536**, 211–215 (2013).
20. C.-W. Chen, S.-Y. Hsiao, C.-Y. Chen, H.-W. Kang, Z.-Y. Huang and H.-W. Lin, *J. Mater. Chem. A* **3**, 9152-9159 (2015).
21. B. G. F. Burkhard, E. T. Hoke and M. D. Mcgehee, *Adv. Mater.* **22**, 3293–3297 (2010).
22. Z. Song, J. Werner, N. Shrestha, F. Sahli, S. De Wolf, B. Niesen, S. C. Watthage, A. B. Phillips, C. Ballif, R. J. Ellingson and M. J. Heben, *J. Phys. Chem. Lett.* **7**, 5114–5120 (2016).
23. K. W. Kemp, A. J. Labelle, S. M. Thon, A. H. Ip, I. J. Kramer, S. Hoogland and E. H. Sargent, *Adv. Energy Mater.* **3**, 917–922 (2013).
24. K. M. Kandil, M. S. Altouq, A. M. Al-asaad, L. M. Alshamari, I. M. Kadad and A. A. Ghoneim, *Smart Grid Renew. Energy* **2**, 375–387 (2011).
25. A. R. Uhl, Z. Yang, A. K.-Y. Jen and H. W. Hillhouse, *J. Mater. Chem. A* **5**, 3214–3220 (2017).